

2D velocity fields of simulated interacting disc galaxies

T. Kronberger^{1,2}, W. Kapferer¹, S. Schindler¹, and B. L. Ziegler^{2,3}

¹ Institut für Astro- und Teilchenphysik, Universität Innsbruck, Technikerstr. 25, 6020 Innsbruck, Austria
e-mail: Thomas.Kronberger@uibk.ac.at

² Institut für Astrophysik, Universität Göttingen, Friedrich-Hund-Platz 1, 37077 Göttingen, Germany

³ Argelander-Institut für Astronomie, Universität Bonn, Auf dem Hügel 71, 53121 Bonn, Germany

Received 23 April 2007 / Accepted 11 July 2007

ABSTRACT

We investigate distortions in the velocity fields of disc galaxies and their use in revealing the dynamical state of interacting galaxies at different redshifts. We model disc galaxies in combined N -body/hydrodynamic simulations. 2D velocity fields of the gas are extracted, which we place at different redshifts from $z = 0$ to $z = 1$ to investigate resolution effects on the properties of the velocity field. To quantify the structure of the velocity field we also perform a kinematic analysis. If the galaxy is undisturbed we find that the rotation curve extracted from the 2D field agrees well with long-slit rotation curves. This is not true for interacting systems, as the kinematic axis is not well defined and in general does not coincide with the photometric axis of the system. For large (Milky way type) galaxies we find that distortions are still visible at intermediate redshifts but are partly smeared out. Thus a careful analysis of the velocity field is necessary before using it for a Tully-Fisher study. For small galaxies (disc scale length ~ 2 kpc) even strong distortions are not visible in the velocity field at $z \approx 0.5$ with currently available angular resolution. Therefore we conclude that current distant Tully-Fisher studies cannot give reliable results for low-mass systems. Additionally we confirm the power of near-infrared integral field spectrometers in combination with adaptive optics (such as SINFONI) to study velocity fields of galaxies at high redshift ($z \sim 2$).

Key words. galaxies: kinematics and dynamics – galaxies: interactions – methods: numerical

1. Introduction

Recently it has become technically feasible to observe the full 2D velocity field (VF) of local galaxies in optical wavebands using integral field units (IFUs) such as SAURON (e.g. Ganda et al. 2006) or Fabry-Perot interferometry (e.g. Chemin et al. 2006; Garrido et al. 2002). For intermediate and high redshift galaxies, however, there are few observational studies of 2D velocity fields available.

Flores et al. (2006) observed the 2D velocity field of 35 galaxies at intermediate redshift ($0.4 < z < 0.75$) using FLAMES/GIRAFFE at VLT. One aspect was to investigate the redshift evolution of the Tully-Fisher relation. A different approach, used by our group, was presented by Ziegler et al. (2006) and Kutdemir et al. (2007) who utilize multiple-object spectroscopy from the VLT with different slit positions on each galaxy to construct the full velocity field for each galaxy. Most of the other studies of distant, faint, and small galaxies are still based on slit spectroscopy (e.g. Vogt 2001; Böhm et al. 2004). To account for distortions and irregularities in the velocity fields is in both cases critical, especially when aiming at a distant Tully-Fisher study. In two recent papers we showed that observational constraints and galaxy-galaxy interactions can severely influence the determination of the rotation curve of observed disc galaxies (Kapferer et al. 2006; Kronberger et al. 2006).

In this paper we investigate to what extent the full 2D velocity field of a galaxy can be used to gain information on its internal kinematics and hence can improve the quality of e.g. Tully-Fisher studies. This question is also important to distinguish between different interaction processes by mapping 2D velocity fields and to study their impact on galaxy evolution. We

focus on the question of how the visibility of distortions depends on the redshift of the observed galaxy, i.e. the actual spatial resolution of the galaxy. We place a galaxy at different redshifts and bin the velocity according to the spatial resolution at that redshift. A similar study for observed galaxies was presented by Epinat et al. (2006).

Additionally to the examination of 2D velocity fields of intermediate redshift galaxies from optical spectroscopy we investigate the performance of near-infrared integral field spectrographs that are used together with adaptive optics. As a prototype we take the characteristics of SINFONI at the Very Large Telescope of the European Southern Observatory to study the velocity fields of galaxies at $z \sim 2$. For example, Genzel et al. (2006) observed the velocity field of a massive protodisc at $z = 2.38$ detecting an ordered rotation without any hint of a major merger event in the system.

Jesseit et al. (2007) analysed 2D velocity fields of simulated galaxies. They focused on simulated disc merger remnants and found that many different kinematical phenomena can be observed in the stellar velocity maps, such as kinematic misaligned discs or counter-rotating-cores. For the analysis they also used the kinematic method of Krajnović et al. (2006) as we do in this paper. However, they did not investigate the redshift dependence of the 2D velocity fields.

The paper is organised as follows. In Sects. 2 and 3, we describe the simulations, the interaction geometries, and the way we extract realistic 2D velocity fields from the numerical data. In Sect. 4 the results for different interaction scenarios and their dependence on the angular resolution are presented. We end with a summary of the main conclusions in Sect. 5.

Table 1. Interaction parameters for the simulations. C2: the two interacting model galaxies. Model galaxy A is a Milky Way type spiral galaxy while model galaxy B represents a small spiral galaxy, with the mass ratio of the two galaxies being 8:1. C7: minimum separation [kpc]; C8: initial relative velocities of the two galaxies [km s^{-1}]. In Col. C9 we give the initial orbital energy of the encounter in Joule.

Simulation	C2	Φ_1	Θ_1	Φ_2	Θ_2	C7	C8	C9
1	A-B	0	0	0	0	50	250	4.8×10^{51}
2	A-B	0	0	0	0	5	250	4.8×10^{51}
3	B-B	0	0	0	0	5	120	9.7×10^{50}
4	A-B	0	0	180	0	5	250	4.8×10^{51}
5	A-B	0	0	90	0	5	250	4.8×10^{51}
6	A-A	0	0	0	0	5	350	1.1×10^{53}

2. Simulations

In this work we use some of the simulated systems presented in Kapferer et al. (2005), which were subsequently used by Kapferer et al. (2006) and Kronberger et al. (2006). The simulations were carried out with the N -body/SPH code GADGET-2 developed by Springel (see Springel 2005, for details). In this code the gas of the galaxies is treated hydrodynamically and prescriptions for cooling, star formation, stellar feedback, and galactic winds are included (Springel & Hernquist 2003). The collisionless dynamics of the dark matter and the stellar component is calculated using an N -body technique. The initial conditions were built according to Springel et al. (2005), based on the analytic work of Mo et al. (1998). The two model galaxies were chosen such that they represent a Milky Way type and a small spiral galaxy, with the mass ratio of the two galaxies being 8:1. Therefore, the total mass of the model galaxies A and B is $1.34 \times 10^{12} h^{-1} M_\odot$ and $1.67188 \times 10^{11} h^{-1} M_\odot$, respectively. The combined N -body/SPH simulation calculates 5 Gyr of evolution. For each time step, we know the velocity of each particle and can hence extract realistic 2D velocity fields of the gas.

Concerning the spatial alignment and impact parameters, we follow the notation introduced by Duc et al. (2000) to describe the interaction geometry. The parameter b corresponds to the minimum separation of the galaxies' trajectories, as if they were point masses on Keplerian orbits. Additionally, two angles, Θ and Φ define the spatial orientation of the disc.

For the complete sample, we selected the alignments in such a way as to cover as many geometries as possible, including minor and major mergers and fly-bys (achieved by increasing the minimum separation). For this analysis we use three different interaction geometries, which we list in Table 1. These three simulations allow us to study different classes of kinematical distortions, detailed in Sect. 3.

Additional important quantities of the simulations, such as the particle numbers, are summarized in Table 2. Throughout the paper we adopt the standard Λ CDM cosmology with $\Omega_\Lambda = 0.7$, $\Omega_m = 0.3$, and $h = 0.7$.

3. Extraction of realistic 2D velocity fields

To construct realistic 2D velocity fields, we project all gas particles of the N -body/SPH simulations onto a Cartesian, equally spaced grid. The spacing is chosen such that the spatial resolution at the assumed redshift of the model galaxy corresponds to the angular resolution of current state-of-the-art observations. For the investigated redshift range from $z = 0$ to $z = 1.0$ we adopt an angular resolution typical for IFU or FPI observations, namely $0.4''$ (e.g. Chemin et al. 2006). The angular resolution of

SAURON, for example, would be $0.3''$ or $0.9''$. For intermediate redshifts we additionally chose $0.25''$, which is the pixel scale along the FORS2 slit as used by Ziegler et al. (2006) and $0.52''$, which is the lenslet size of FLAMES/GIRAFFE at VLT (e.g. Flores et al. 2006). We calculate for each redshift the physical resolution according to the given angular resolution using the concordance cosmological model (see Table 3). The velocity field of the galaxy is binned using this spatial resolution.

From the knowledge of the full 3D velocity fields and the interaction history of the galaxies in our simulations we define three kinematical classes, in principle analogous to classifications in Flores et al. (2006) or Krajnović et al. (2006):

- **Undisturbed rotation:** the galaxy is not interacting and the rotation curve has the “classical” shape, rising in the inner part and turning into a flat regime.
- **Disturbed rotation:** rotation is still predominant but disturbed by a minor interaction, e.g. a minor merger event. Non-rotational components of the velocity field are also clearly visible as peculiarities in 1D rotation curves (Kronberger et al. 2006).
- **Distorted velocity field:** the velocity field is heavily distorted by a strong merger event, i.e. an interaction with a galaxy of similar or higher mass. It shows a very complex pattern and no longer has a regular rotation curve.

The main question that we investigate in this paper is how such classifications depend on the redshift of the observed galaxy, i.e. the actual spatial resolution of the galaxy. In this context the seeing plays a crucial role, as it typically exceeds the angular resolution of the instrument. To simulate seeing effects on our velocity-field measurements, a convolution with a Gaussian point spread function was applied. We adopted a value of $0.8''$ for the $FWHM$ of the Gaussian seeing, which is a typical value for ground based observations (see e.g. Jäger et al. 2004). The appearance of the velocity fields is therefore dominated by the seeing. Note that we do not calculate an evolution of properties of the galaxy with redshift but study how a given kinematical state of a galaxy is observed at different redshifts.

The studies mentioned above are mainly seeing dominated. We additionally study the possibility of identifying mergers at high redshift ($z \sim 2$) with an adaptive optics instrument such as SINFONI at the VLT. For this investigation we adopt an angular resolution of $0.15''$ as achieved by Genzel et al. (2006).

4. Results

In the subsequent sub-sections we will systematically investigate velocity fields from each of the kinematical classes defined in Sect. 3. The focus lies on the visibility of kinematical distortions as a function of redshift. In order to quantify the distortions and to interpret the partly complex structures in the velocity fields we use the kinemetry package of Krajnović et al. (2006). This analysis is based on the assumption that the mean velocity along best fitting ellipses can be reproduced by a cosine law, i.e.

$$V(a, \Psi) = V_0 + V_c(a) \cos \Psi, \quad (1)$$

where a is the length of semi-major axis of the ellipse, Ψ for discs is the azimuthal angle measured from the major axis in the plane of the galaxy. Note that in general a simple sine correction for the inclination of the disc is applied in observations too. The velocity fields presented here have not been corrected in this way as all of them were extracted at the same inclination $i = 35^\circ$ (except for those presented in Sect. 4.4).

Table 2. Particle numbers, mass resolution and gravitational softening used for the two model galaxies. Additionally the circular velocity of the halo at r_{200} and the disc scale length of the initial conditions are given.

	Particle number	Mass resolution [$h^{-1} M_{\odot}/\text{particle}$]	Softening length [$h^{-1} \text{kpc}$]	Halo circular velocity [km s^{-1}]	Radial disc scale length [$h^{-1} \text{kpc}$]
Galaxy A:					
Dark matter halo	30 000	4.2×10^6	0.4	160	
Disk collisionless	20 000	3.3×10^5	0.1		
Gas in disk	35 000	8.4×10^4	0.1		4.5
Galaxy B:					
Dark matter halo	30 000	5.3×10^5	0.4	80	
Disk collisionless	20 000	4.2×10^4	0.1		
Gas in disk	35 000	1.1×10^4	0.1		2.25

Table 3. Physical resolution according to 1 arcsec angular resolution for different redshifts in the standard Λ CDM cosmology.

Redshift	Physical resolution according to $1''$ [kpc]
0.05	0.98
0.1	1.85
0.2	3.30
0.3	4.46
0.4	5.38
0.5	6.11
0.8	7.51
1.0	8.01
2.0	8.38

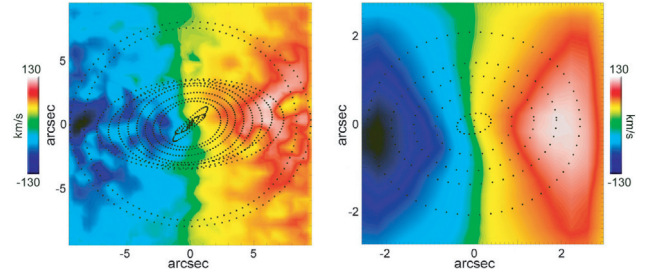
The position angle Γ and the axial ratio ($q = b/a$) of the ellipses are calculated as a function of radius from the galactic centre. Deviations from that cosine law are measured using an harmonic expansion along the ellipses, i.e.

$$V(a, \Psi) = \sum_{n=1}^N k_n(a) \cos[n(\Psi - \phi_n(a))], \quad (2)$$

where ϕ is the phase coefficient. Higher order Fourier terms and radial changes of Γ or q are used to quantize deviations in the velocity field from a simple rotation. There is an intrinsic relation of the surface brightness of the galaxy and the line-of-sight velocity. Both are moments of the underlying distribution function, where the surface brightness is the zeroth order moment and the line-of-sight velocity is the first order moment. Note, however, that for gas, as in our case, the situation is different from collisionless stellar systems, where the distribution function for simplified systems can be calculated analytically. As we deal here mostly with rotating disc-like structures, the use of ellipses is a natural choice. For distorted and elliptical systems this assumption will be violated and the deviation is quantified by the Fourier analysis. In principle the calculation of the best fitting ellipses works in a two step approach as follows. First, higher order terms are minimized, which, according to their analysis, do not carry the major contribution to the map. This happens on a grid of position angles (Γ) and flattenings (q) and leads to initial values (Γ_{\min}) and (q_{\min}) for a second fit. In this second fit all parameters of the ellipse are taken into account and the Fourier analysis can be performed to arbitrary order. For more details on the algorithm see Krajnović et al. (2006).

4.1. Undisturbed velocity fields

We investigate the simple case of an undisturbed spiral galaxy, i.e. an example of the first kinematical class presented in Sect. 3.

**Fig. 1.** 2D velocity field of an undisturbed modelled disc galaxy as seen at redshift 0.1 (*left*) and at 0.5 (*right*). Overlaid as contours are the best fitting ellipses from the kinemetry analysis.

This class is particularly important for Tully-Fisher studies, as only for these galaxies is the maximum rotational velocity V_{\max} an approximation of the virial mass of the system. For this investigation we use galaxy A in simulation 1 (see Table 1), at a point when the two galaxies are still well separated. The adopted inclination of the galaxy is 35° (90° is defined to be edge-on). The velocity field is very regular at all redshifts. The appearance of our VFs is dominated by seeing, as we adopted a constant value of $0.8''$ for the *FWHM*, which is always larger than the angular resolution we use. Both effects, the worse sampling at higher redshifts and the large seeing blur the velocity field when shifted to higher z . In Fig. 1 we present the VFs of an undisturbed disc galaxy as seen at two different redshifts ($z = 0.1$ and $z = 0.5$). Overlaid on the VF are the best fitting ellipses from the kinematic analysis. At a redshift of 0.1 there is some structure visible in the VF, e.g. a small twist of the position angle Γ towards the centre. Some fluctuations of the rotational velocity are present in the disc. These small structures in the VF are completely blurred at redshift $z = 0.5$.

Quantitatively the differences can be seen in Fig. 2 in the radial profiles of the kinematic properties, calculated using the kinemetry programme. The program also calculates formal 1σ errors from the covariance matrix, which are shown as error bars in the plots. These uncertainties are estimated from the measurement uncertainties in the kinematic data. As we do not account for the spectral resolution of the instruments, we use the scatter of the velocity field. Note that this is just a formal uncertainty, which in reality is higher, also because systematic errors add up.

While at $z = 0.1$ both Γ and q show variations with radius, they are almost constant at $z = 0.5$. The first order moment k_1 corresponds to the rotation curve (RC) of a spiral galaxy or more generally to the bulk motion in the velocity field. For the undisturbed velocity field presented here it shows typical behaviour of a rotation curve, i.e. rising in the inner part and flattening at

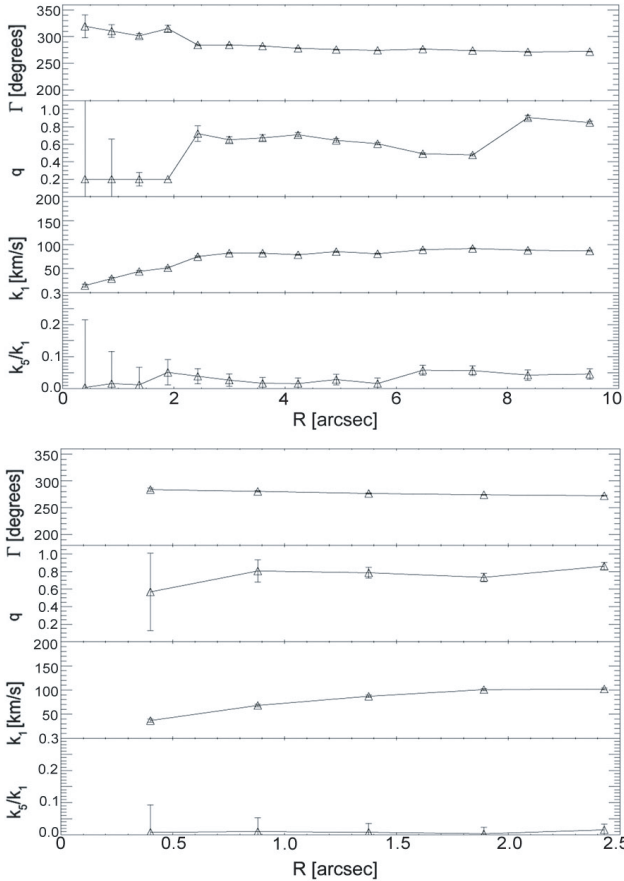


Fig. 2. Radial profiles of the kinematic properties, calculated using the kinemetry programme for an undisturbed Milky Way type galaxy at redshift $z = 0.1$ (top) and $z = 0.5$ (bottom). The position angle Γ and the flattening q of the best fitting ellipses as well as the first and the fifth order Fourier terms k_1 and k_5 are plotted as a function of radius.

larger radii. This undisturbed shape is present at redshift $z = 0.1$ and at $z = 0.5$. In Fig. 3 we show the rotation curves of the system at redshift $z = 0.5$ obtained from the 2D velocity field (triangles) and from a simulated slit (asterisks), extracted as described in Kronberger et al. (2006). The modelled slit was placed over the major axis of the galaxy with a slit width of $1''$. The RCs extracted in these different ways agree very well, as expected for such a regular velocity field. We plot in the same figure as a dashed line the RC extracted at redshift $z = 0.1$, which agrees reasonably well with the higher redshift RCs. This demonstrates the principle power of 2D velocity fields for distant Tully-Fisher studies *if* regular, undisturbed velocity fields are considered.

The last row in Fig. 2 shows a quantitative measure for distortions in the 2D velocity field. The fifth order term of the harmonic expansion k_5 represents complex, kinematically separate components in the velocity field. In the plot the ratio k_5/k_1 is shown. For the regular VF presented in this section, this ratio is small, generally below 0.1 for all redshifts. However, this value is very sensitive to the resolution of the velocity field. While at $z = 0.1$ there are some radii with increased k_5/k_1 , these signatures are completely smeared out at higher redshifts. At $z = 0.5$ the ratio is almost constant below a value of 0.02. This indicates problems with identifying distortions in 2D velocity fields at higher redshifts. This issue will be addressed in the next section.

At redshift $z = 0.5$ we study the effects of angular resolution on VF properties by considering in addition to the standard angular resolution of $0.4''$ two more values. We adopt the $0.25''$ of

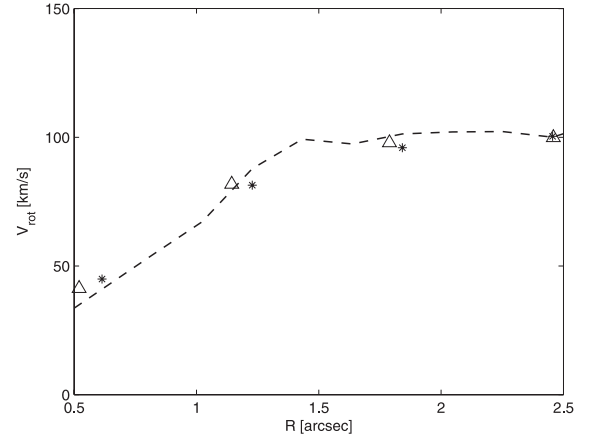


Fig. 3. Rotation curves of the isolated galaxy extracted from the 2D velocity field (triangles) and using a modelled slit (asterisks) at redshift $z = 0.5$. The dashed line shows the corresponding RC at redshift $z = 0.1$ obtained from a modelled slit.

Ziegler et al. (2006) in their sample using FORS2 spectroscopy and $0.52''$ as for FLAMES/GIRAFFE at VLT (e.g. Flores et al. 2006). At the FLAMES/GIRAFFE angular resolution the VF is even more smeared out than at $0.4''$ resolution. However, the radial behaviour of the kinematic parameters is only slightly affected. The RCs and their maximum value V_{\max} agree reasonably well for all three angular resolutions. Again, with respect to subsequent sections, we point out that this holds only for regular velocity fields.

4.2. Disturbed rotation

In Sect. 3 we defined the kinematical class “disturbed rotation” as a rotating system with a clearly visible distortion. As an example of this class we investigate a model galaxy undergoing a minor merger (simulation 2). At this snapshot the distance between the two galaxies is smaller than the radius of galaxy A, i.e. galaxy B encounters the Milky Way type galaxy A in its first passage. The small galaxy permeating the more massive galaxy A is clearly visible in the velocity field, as an irregular structure in the lower right part of the VF presented in Fig. 4. At redshift $z = 0.1$ the kinemetry analysis shows strong variations of the position angle Γ and the flattening q with radius (see Fig. 5). The radial fluctuations are stronger than for the isolated galaxy. The first order Fourier term k_1 , which corresponds to the rotation curve, also shows distortions and the ratio k_5/k_1 is significantly higher than in the isolated case. The shape and the maximum value of the RC are different to the regular RC. Therefore, this galaxy could not be used for Tully-Fisher studies. RCs extracted from this galaxy with a slit show clear signatures of distortion (Kronberger et al. 2006), especially an asymmetric shape with a rising side pointing towards the interaction. However, with 2D velocity fields the nature of the interaction becomes more accessible. The almost undistorted left hand side of the VF points towards a very asymmetric interaction, which suggests tidal interaction. This asymmetry is less visible at $z = 0.5$, where the distortion is smeared out. Visual assessment might lead to a misclassification as “undisturbed rotation”. However, in a more detailed comparison with Fig. 1 some differences are clearly visible. The most striking difference is the presence of a clear kinematic axis in the regular VF, which is not present in Fig. 4.

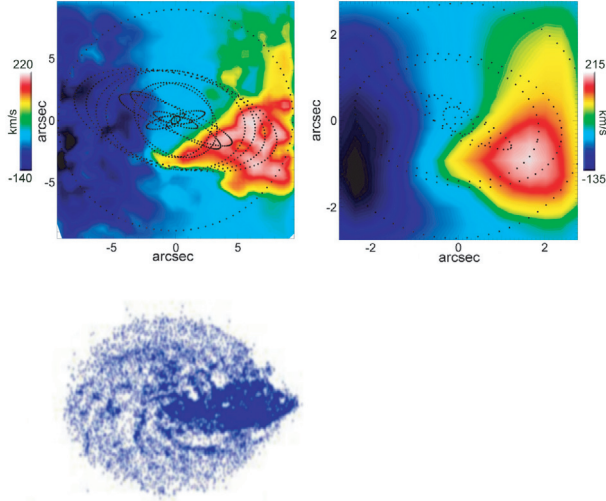


Fig. 4. 2D velocity field of a modelled Milky Way type disc galaxy disturbed by an ongoing minor merger event (i.e. the small galaxy B is permeating galaxy A in its first passage) as seen at redshift 0.1 (*top left*) and 0.5 (*top right*). Overlaid as contours are the best fitting ellipses from the kinemetry analysis. In the lower panel the projected gas distribution at this timepoint is shown to illustrate the interaction geometry.

We present the rotation curve extracted from the 2D velocity field and using a simulated slit in Fig. 6. In contrast to the case of the isolated galaxy, the RCs differ significantly in the interacting system. The reason for this difference is the fact that in an interacting system the kinematic axis is not well defined and in general does not coincide with the photometric axis of the system. Thus, the slit in general does not follow the kinematic axis of the galaxy. Only the knowledge of the full 2D velocity field allows one to determine the kinematic axis.

The plots of the radial behaviour of the kinemetry parameters in Fig. 5 do not yield clear evidence for a distorted VF at $z = 0.5$. Only the outermost data point of k_5/k_1 shows a significant increase. The situation is even worse for the resolution obtained with FLAMES/GIRAFFE. Although the maximum rotational velocity of the RC becomes similar to the one of the isolated galaxy due to the smearing out of the VF, a misclassification as an undistorted galaxy would result in systematic errors in Tully-Fisher studies. The luminosity of the system is possibly enhanced due to a merger-induced starburst.

In Fig. 7 we show the 2D velocity field of this example for redshift $z = 0.05$, $z = 0.3$, $z = 0.8$, and $z = 1.0$. It is clearly visible how substructures are blurred at higher redshift.

We studied the effects of different interaction geometries on the results presented above. We considered a counter-rotating unequal mass merger (simulation 4) and an unequal mass merger, where the disc of galaxy B is initially perpendicular to the disc of galaxy A (simulation 5). The appearance of the velocity fields does differ for the different interaction scenarios. However, the main conclusions drawn so far do not change. The merger is clearly visible in the asymmetric shape of the velocity field, the distortions are, however, blurred at higher redshift.

It is more probable to observe an interacting system in a pre- or post merger phase than in the relatively short period where the two galaxies are merged. Therefore, we study the same system 100 Myr after the direct encounter described above, i.e. after the first pericentre passage. This is the period between the first passage and the complete merging of the two galaxies. The small

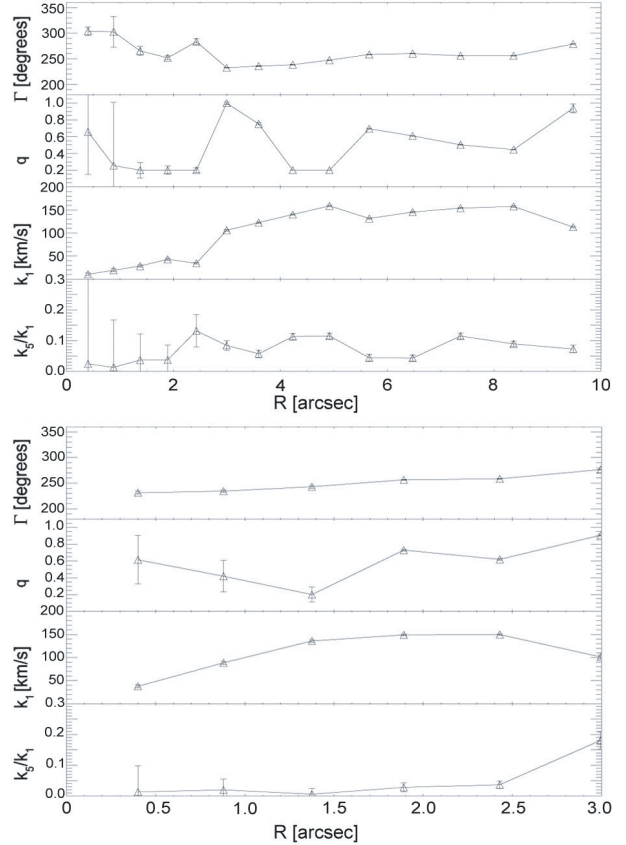


Fig. 5. Radial profiles of the kinemetric properties, calculated using the kinemetry programme for the interacting galaxy A of Fig. 4 (minor merger) at redshift $z = 0.1$ (*top*) and $z = 0.5$ (*bottom*). The position angle Γ and the flattening q of the best fitting ellipses as well as the first and the fifth order Fourier terms k_1 and k_5 are plotted as a function of radius.

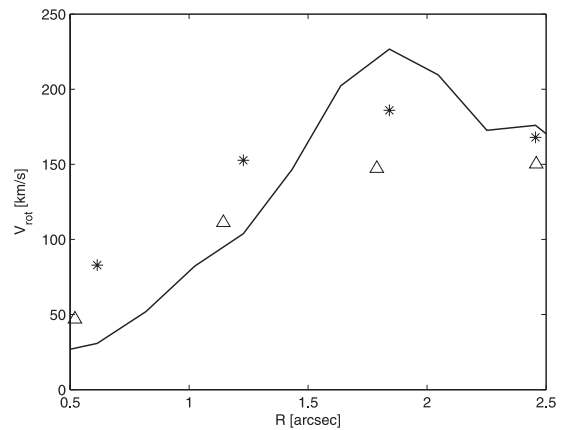


Fig. 6. Rotation curves of the interacting galaxy extracted from the 2D velocity field (triangles) and using a modelled slit (stars) at redshift $z = 0.5$. The solid line shows the corresponding RC from the 2D field at redshift $z = 0.1$.

galaxy went through the gaseous disc of the massive galaxy and left a disturbed velocity field. In the direct image the interaction is no longer visible at redshift $z = 0.5$. In Fig. 8 we show the distribution of the stellar mass in the galaxy as a 2D image and as a radial profile. By assuming a certain constant mass-to-light ratio this could be translated to a light distribution. The profile can be fitted by an exponential law. The velocity field still shows

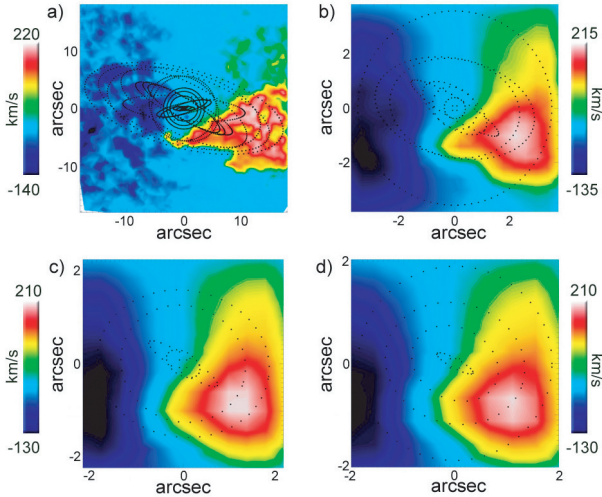


Fig. 7. Evolution of the 2D velocity field appearance with redshift: **a)** $z = 0.05$, **b)** $z = 0.3$, **c)** $z = 0.8$, **d)** $z = 1.0$. Overlaid as contours are the best fitting ellipses from the kinemetry analysis. $z = 0.1$ and $z = 0.5$ are shown in Fig. 4.

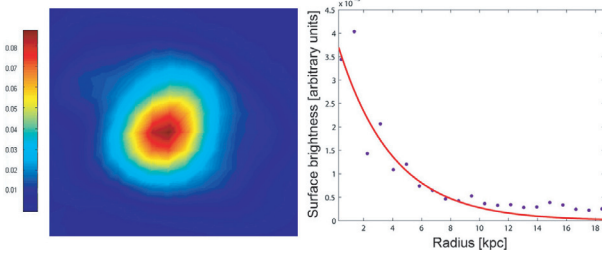


Fig. 8. The distribution of the stellar mass in the galaxy as 2D image (*left*) and as a radial profile (*right*), which translates under an assumption of a constant mass-to-light ratio to a surface brightness profile. The galaxy is shown 100 Myr after the first pericentre passage of galaxy B at a resolution corresponding to an artificial redshift of $z = 0.5$. The exponential fit to the profile is shown as a red line. The physical field of view of the 2D image is 36×36 kpc.

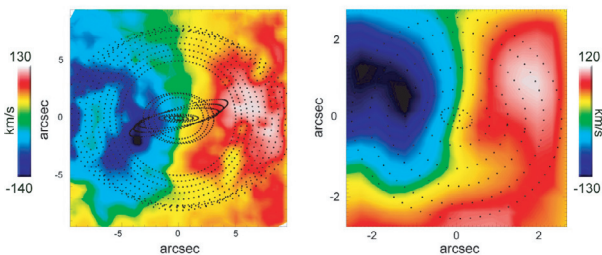


Fig. 9. 2D velocity field of a modelled disc galaxy 100 Myr after a minor merger event as seen at redshift 0.1 (*left*) and 0.5 (*right*). The best fitting ellipses from the kinemetry analysis are overlaid as contours.

some signatures of the interaction (see Fig. 9) at lower redshift but at $z = 0.5$ these are heavily smeared out. Thus, the velocity information is an important complement to the morphological analysis when studying interactions of galaxies but only if the VF is sufficiently sampled.

Kinematic disturbances from interactions are expected to fade within a few rotation cycles (≤ 1 Gyr e.g. Dale et al. 2001; Kronberger et al. 2006). Only 200 Myr after the direct encounter presented above neither the direct image nor the VF show clear signatures of the interaction any longer. In a more detailed analysis, however, signs of the interaction can still be

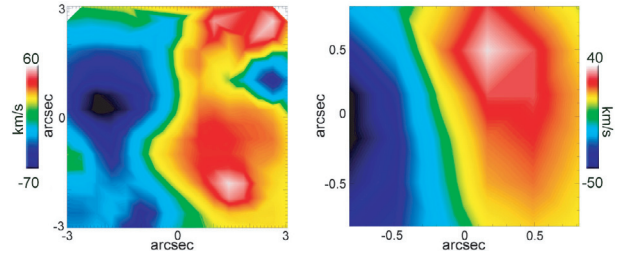


Fig. 10. 2D velocity field of a model galaxy B disturbed by an equal mass merger, 300 Myr after the first pericentre passage of the two galaxies, as seen at redshift 0.1 (*left*) and 0.5 (*right*).

found. About 1 Gyr after the first passage, when both galaxies are well separated but approaching each other again, galaxy A would be classified as undisturbed, even when observed at low redshift.

The analysis so far was made for the rather large galaxy A, which has a radial scale length of about 4.5 kpc. Therefore, the velocity field is sampled by many pixels. The situation is completely different for smaller galaxies, e.g. model galaxy B. We investigate a “disturbed rotation” of galaxy B using a snapshot of simulation 3, an equal mass merger of two small galaxies B. Equal mass mergers massively disturb the velocity field of the gas of the interacting galaxies. Most of the gas is converted into stars by a merger-induced starburst or lost to the intergalactic medium by tidal forces (e.g. Kapferer et al. 2005). We choose a snapshot about 300 Myr after the first encounter, when again some regular rotation has been established.

In Fig. 10 the 2D velocity field of the galaxy for this snapshot is shown at redshift $z = 0.1$ and at $z = 0.5$ with an angular resolution of $0.4''$. While at $z = 0.1$ the distortions in the VF are clearly visible, they are completely smeared out at $z = 0.5$ leaving a regular VF that would be classified as “undisturbed rotation”. This classification is supported by the radial behaviour of the kinematic quantities shown in Fig. 11, although at $z = 0.5$ only two ellipses were fitted due to the small number of available pixels. Such undetected distortions introduce an enormous source of systematic errors in distant Tully-Fisher studies. Therefore we conclude that current distant Tully-Fisher studies cannot give reliable results for low-mass systems if the velocity field is not sampled sufficiently.

In Fig. 12 we present the 2D velocity field of galaxy B for redshift $z = 0.05$, $z = 0.2$, $z = 0.3$, and $z = 0.4$. Gradually the distortions are blurred, leaving an almost regular VF at $z = 0.4$. We investigate how long the 2D velocity field maintains the disturbed features. After the first pericentre passage of the two galaxies the velocity field settles again to an undisturbed state. As for the unequal mass merger discussed above, the strongest features disappear after several hundred Myr while an undisturbed velocity field is again present after about 1 Gyr. Note that in this period the two galaxies are approaching each other again for their second passage, but still without any direct interaction yet.

We also investigate a major merger between two large galaxies A where the velocity field spreads over more pixels. In this case the situation is, as expected, slightly clearer than for the small galaxy B. Especially for the kinematical analysis more ellipses can be fitted even at redshift $z = 0.5$. Nevertheless a similar trend is observed as for galaxy B. While the distortions are clearly visible at low redshift, they are subsequently smeared out when the galaxy is placed at higher redshift. In Fig. 13 we show the 2D velocity field and the radial profiles of the kinematic

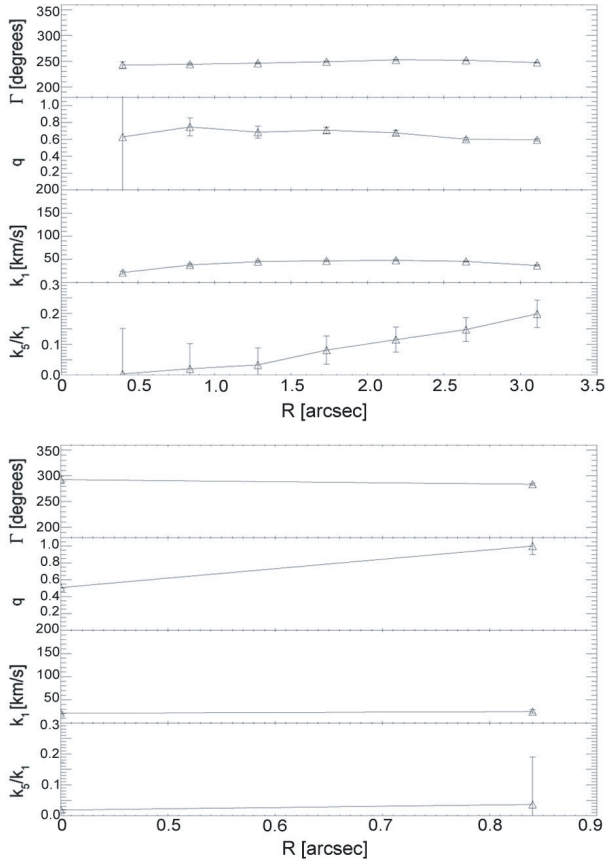


Fig. 11. Radial profiles of the kinematic properties, calculated using the kinemetry programme for galaxy B 300 Myr after an equal mass merger for redshift $z = 0.1$ (top) and $z = 0.5$ (bottom). The position angle Γ and the flattening q of the best fitting ellipses as well as the first and the fifth order Fourier terms k_1 and k_5 are plotted as a function of radius.

properties as seen at redshift $z = 0.5$ for model galaxy A disturbed by an equal mass merger, 100 Myr after the first passage of the two discs. The appearance of the velocity field and the radial behaviour of mainly the flattening q point towards an interaction (compare to Figs. 1 and 2 for the undisturbed case). Small-scale distortions, however, are smeared out.

Complementary to these investigations of VFs at intermediate redshift, we study the appearance of the 2D velocity field at $z = 2$ as observed with SINFONI at VLT. Due to the use of adaptive optics, these observations are not seeing limited and have a high angular resolution (we adopt $0.15''$ for our study). As a test case we take galaxy A during an ongoing minor merger in simulation 2. The velocity field of this timepoint for seeing limited observations and various redshifts is shown in Fig. 7. The galaxy has a radial exponential disc scale length of 4.5 kpc and is therefore comparable in size to the one observed by Genzel et al. (2006). The velocity field of this timepoint as seen at redshift $z = 2$ with an instrument such as SINFONI is presented in Fig. 14. Peculiarities in the VF caused by the merger are clearly visible.

4.3. Distorted velocity field

To heavily disturb the velocity field of a spiral galaxy, a tidal interaction with a galaxy of similar or higher mass is necessary. In this section we use the velocity field of the small galaxy B in

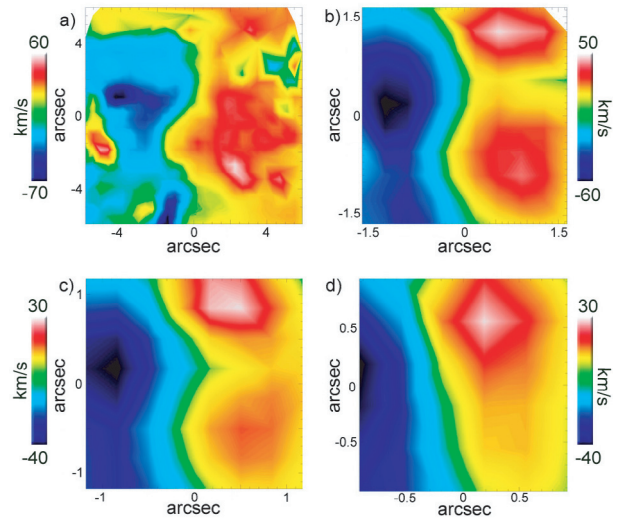


Fig. 12. Evolution of the 2D velocity field appearance with redshift of a model galaxy B disturbed by an equal mass merger, 300 Myr after the encounter: **a)** $z = 0.05$, **b)** $z = 0.2$, **c)** $z = 0.3$, **d)** $z = 0.4$. Additionally the same 2D velocity fields as seen at $z = 0.1$ and $z = 0.5$ are shown in Fig. 10

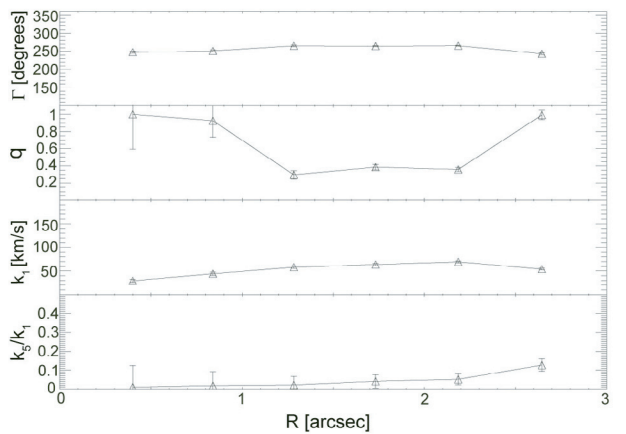
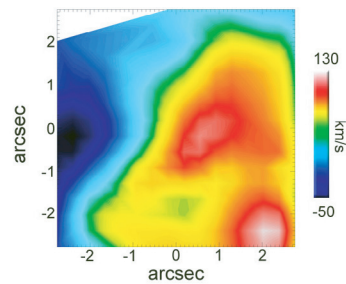


Fig. 13. The 2D velocity field of a model galaxy A disturbed by an equal mass merger, 100 Myr after the first passage of the two discs is shown in the upper panel. The lower panel shows the radial profiles of the kinematic properties, calculated using the kinemetry programme. The position angle Γ and the flattening q of the best fitting ellipses as well as the first and the fifth order Fourier terms k_1 and k_5 are plotted as a function of radius. Both figures correspond to redshift $z = 0.5$.

simulation 2 after its first passage through galaxy A, i.e. about 200 Myr after the first encounter.

In this case the VF no longer shows a regular pattern of rotation. Both at low and intermediate redshift the irregularity is visible, although at $z = 0.5$ the substructure is completely blurred leaving a single “velocity blob” (see Fig. 15). The poor resolution of only 5×5 pixels at this redshift together with the

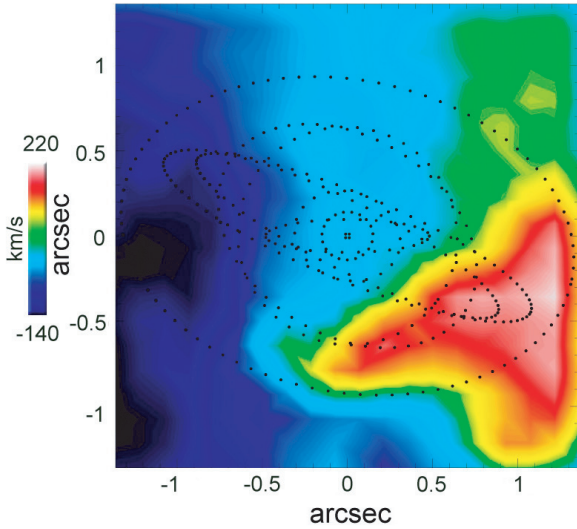


Fig. 14. 2D velocity field of a modelled disc galaxy disturbed by an ongoing minor merger event as seen at redshift 2 using SINFONI at VLT. Overlaid as contours are the best fitting ellipses from the kinemetry analysis.

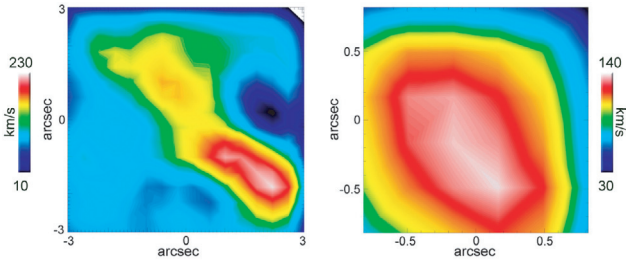


Fig. 15. 2D velocity field of a model galaxy B heavily disturbed by a merger with galaxy A (200 Myr after the first passage through the disc of galaxy A) shown at redshift 0.1 (left) and 0.5 (right).

seeing is the reason for this. The better resolution of $0.25''$ does not improve this image significantly. Such a galaxy could not be used for a Tully-Fisher study and could not be mistaken as undisturbed. The plots of the radial behaviour of the kinematic parameters clearly reflect the distortions in the VF. Due to the low number of pixels at intermediate redshifts we constructed this plot only for low redshifts. Figure 16 shows the kinematic parameters at $z = 0.1$. A significant change of the position angle Γ coincides with a large peak in the ratio k_5/k_1 of about 3. Such a correlation between the position angle and k_5/k_1 was also reported and discussed by Krajnović et al. (2006).

The question arises for this interaction scenario of how long the 2D velocity field maintains the severely distorted shape. We found that in this case the distortions of the velocity field are so strong that at no point between the first passage and the final merging could the galaxy be classified as “disturbed” or even “regular” any longer. Before the first pericentre passage the galaxy features an undisturbed rotation, which is increasingly disturbed when the tidal forces of galaxy A become stronger. Once galaxy B passes the Milky Way-type galaxy, the velocity field is heavily distorted, as discussed above.

4.4. Discussion of observational biases

Throughout the paper we have assumed that the velocity field of the galaxy is always observable out to four disc scale lengths,

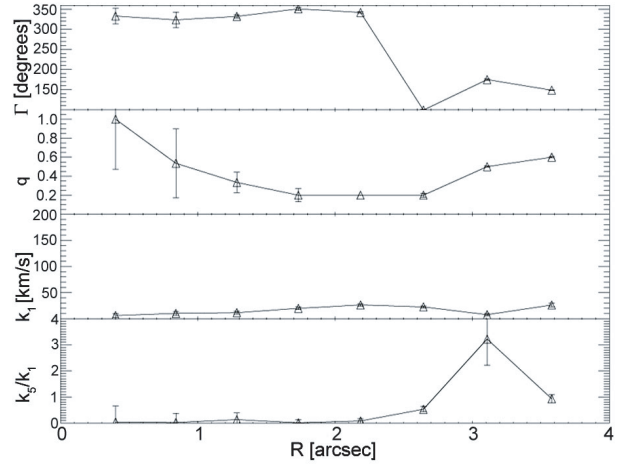


Fig. 16. Radial profiles of the kinematic properties, calculated using the kinemetry programme for galaxy B 200 Myr after a major merger with galaxy A for redshift $z = 0.1$. The position angle Γ and the flattening q of the best fitting ellipses as well as the first and the fifth order Fourier terms k_1 and k_5 are plotted as a function of radius.

which in real observations is, due to limited sensitivity, not always possible. Therefore, depending on the instrument, one might only observe the inner parts of the VF. As a consequence, distortions in the outskirts can be missed. Here we were interested in the principle effects of limited resolution on the appearance of the 2D velocity fields, without specifying a special instrument, i.e. for an idealized observation. In a future work we will study flux-limited velocity fields for special instruments for comparison with observed data.

A second parameter that changes the appearance of the 2D velocity field is the inclination of the galaxy. Throughout the paper we have adopted an inclination $i = 35^\circ$. For an undisturbed galaxy a correction with the sine of the inclination typically is applied to the rotation curve. The appearance of a regular 2D field is not severely affected by inclination. In the case of an interacting galaxy, however, the appearance of the velocity field changes with inclination. A systematic investigation of the effects of inclination is, however, difficult, as they depend on the specific interaction geometry. We sketch here the influence of inclination on the VF presented in Sect. 4.2. Instead of $i = 35^\circ$, we now choose $i = 80^\circ$, i.e. nearly edge-on. The unequal mass edge-on merger of simulation 2 produces VF distortions mainly in the plane of the disc. These distortions are therefore clearly visible at low inclinations, see Fig. 4 but are less prominent for higher inclinations. In Fig. 17 we show the same snapshot as in Fig. 4 but at an inclination of $i = 80^\circ$ instead of $i = 35^\circ$. At $z = 0.5$ the VF even appears regular, hence the interaction might not be recognized.

4.5. Implications for distant Tully-Fisher studies

Many recent studies have analysed the luminosity evolution of galaxies via the Tully-Fisher relation (e.g. Ziegler et al. 2003; Böhm et al. 2004; Bamford et al. 2005; Nakamura et al. 2006; Flores et al. 2006). Some of these studies also focused on environmental effects, i.e. differences in the Tully-Fisher relation between the field and cluster population. Ziegler et al. (2003) and Nakamura et al. (2006) find no significant differences between field and cluster galaxies, whereas Bamford et al. (2005) claim that galaxies in clusters are on average brighter than their field counterparts. The Tully-Fisher relation (TFR) is also

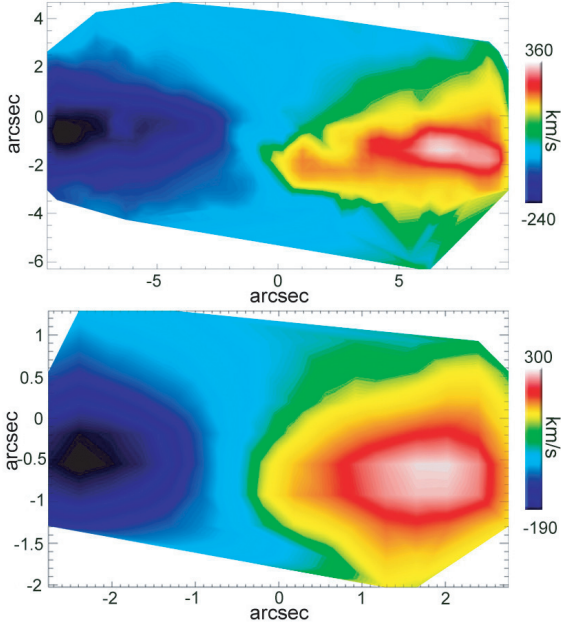


Fig. 17. 2D velocity field of a modelled disc galaxy disturbed by an ongoing minor merger event at redshift 0.1 (*top*) and 0.5 (*bottom*). In contrast to Fig. 4 the inclination in this figure is $i = 80^\circ$.

extensively used as a test case for galaxy formation models. Portinari & Sommer-Larsen (2007) investigated the redshift evolution of the Tully-Fisher relation in cosmological simulations. They find an offset between the observed and simulated Tully-Fisher relation at $z = 0$. The evolution they find is intermediate between diverse observational results. Parts of the discrepancies between the various observational results may be attributed to the way distortions in the velocity fields of the galaxies are accounted for.

The results from this work suggest that galaxies from an observed sample that are misclassified as undisturbed can introduce a systematic error in the Tully-Fisher diagram. A Tully-Fisher analysis assumes that the galaxies are in virial equilibrium, which is revealed by a smooth, regular and symmetric rotation curve that rises rapidly in the inner part and flattens in the outer part. This “flat” or maximum circular velocity is one parameter of the TFR, the other being the luminosity. In a disturbed system, the measured V_{\max} is no longer an accurate estimate for the virial velocity of the halo and, hence, not a good proxy for the total mass of the system. Also, the amount of luminosity of the galaxy is influenced by the interaction (see Kapferer et al. 2005). To what extent both quantities are affected by the interaction depends on the interaction geometry and the time.

Therefore, if distortions or peculiarities are visible in the RC, the galaxy would not be included in a TF analysis. However, in this study, we have shown that at intermediate redshifts, due to lack of resolution, signatures of an interaction are blurred, so that a distorted galaxy mimics a regular one in several cases. If such disturbed (but unrecognized) systems are used in a Tully-Fisher study, the scatter will be significantly increased. In contrast to slit observations of a one-dimensional RC, the availability of a two-dimensional VF allows a much better assessment of irregularity. Nevertheless, in the case of a small and faint galaxy, where the VF spreads over a few pixels only, an interaction could be missed as well. The inclusion of such intrinsically disturbed objects could therefore mimic an evolution at the faint end of the Tully-Fisher relation.

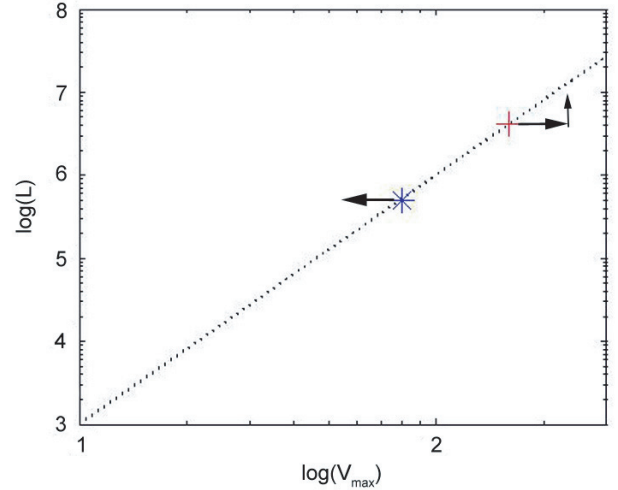


Fig. 18. Position of the two undisturbed model galaxies in the luminosity-rotational velocity plane (red cross: galaxy A; blue asterisk: galaxy B). The two galaxies lie on a Tully-Fisher relation with slope 3 (dotted line), consistent with observations of local galaxy samples. The arrows indicate the trends in which way the interactions studied in this work change the positions of the galaxies. For the Milky Way type galaxy, the investigated interaction is the minor merger with galaxy B, while for model galaxy B it is the major merger case with a second galaxy B. These trends can be observed at all redshifts but with different strengths.

We show in Fig. 18 how a galaxy moves in the Tully-Fisher diagram if V_{\max} values are used that do not correspond to the virial velocity. First, we place the undisturbed galaxies onto the TFR under the assumption of a constant mass-to-light ratio. The simulated Milky Way galaxy A and the less massive galaxy B then follow a linear relation with slope of 3, i.e. $L \propto V_{\max}^3$. This is in good agreement with observed local values. Pierce & Tully (1992) obtain a value of 2.99 for their sample, other authors obtain values between 2.96 and 3.2 (see Ziegler et al. 2002, and references therein). In Fig. 18 we show how interactions change the positions of the galaxies. Note that these trends are taken from the interaction scenarios studied in this work. Other interaction geometries or times might lead to a different effect. The Milky Way type galaxy A moves to the right, if the minor merger presented in Sect. 4.2 is not recognized. As the interaction also triggers star formation, the luminosity increases at the same time. In the case studied here, the effect on V_{\max} is greater than the brightening of the galaxy. For the small galaxy B, in the case of a major merger the interactions lead to an underestimation of the true V_{\max} . At the same time, the luminosity stays roughly constant or even decreases by a small amount, as stars are lost by the merger. Assuming that this trend holds more generally and that distortions are more easily missed at higher redshift for small galaxies, this effect could mimic a luminosity evolution at the faint end of the Tully-Fisher relation. Therefore, a careful analysis is necessary to prevent the inclusion of disturbed systems in distant Tully-Fisher studies.

5. Summary and conclusions

We have investigated 2D velocity fields of isolated and interacting spiral galaxies using N -body/SPH simulations. We focused on the question of how the full 2D velocity field of a galaxy can be used to gain information on its internal kinematics. This

issue was analysed with special emphasis on distant Tully-Fisher studies.

- We found that with the help of 2D velocity fields the nature of the interaction becomes more accessible than with rotation curves from simple long-slit spectroscopy. Quantitative analyses such as harmonic expansion, which is, for example, used by the kinemetry package of Krajnović et al. (2006), offer an additional possibility to identify distortions in a VF.
- Tidal interactions lead to an asymmetric velocity field, where the side pointing to the interaction is disturbed while the side remote from the interaction stays relatively unaffected. This behaviour can also be found in the rotation curve of the system (Kronberger et al. 2006).
- By shifting the VF artificially to higher redshifts we found that, although small-scale structures in the VF are blurred, distortions are still visible at intermediate redshifts for large galaxies. In the case of small galaxies even strong distortions are not visible in the velocity field at $z \approx 0.5$ with currently available angular resolution.
- Severely distorted kinematics, i.e. velocity fields with no or just a small rotational component are also identifiable for small galaxies at intermediate redshift. Thus they should not be mistaken as undisturbed.
- If the galaxy is undisturbed, the quantities derived from the velocity field, e.g. the maximum rotational velocity V_{\max} , do not show systematic variations with resolution and are therefore useable for Tully-Fisher studies.
- We showed that with the help of adaptive optics near-infrared spectrographs (e.g. SINFONI) it is possible to study the internal kinematics of galaxies even at high-redshift ($z \sim 2$), if the observed flux is sufficient to construct a 2D velocity field. Ongoing merger events are then clearly visible in the VF.
- Disturbed velocity fields settle again to a relaxed state after about 1 Gyr. However, after several hundred Myr the distortions can become damped such that a misclassification as “undisturbed rotation” is possible at higher redshifts.
- With the assumption of a constant mass-to-light ratio, we showed that the undisturbed model galaxies lie on a Tully-Fisher relation with a slope of -3 , which is consistent with observations of local galaxy samples. Using systems with unrecognized distortions for a Tully-Fisher study will significantly increase the scatter in the observed relation. As it is more likely that an interaction is missed for small, faint galaxies, the inclusion of disturbed systems can mimic evolution in the faint end of the Tully-Fisher relation.

Acknowledgements. We thank the anonymous referee for fruitful comments which improved the quality of the paper. The authors would like to thank Volker Springel for providing them with GADGET2 and his initial-conditions generator and Davor Krajnović for his Kinemetry software. Thomas Kronberger is a recipient of a DOC fellowship of the Austrian Academy of Sciences. The authors further acknowledge the UniInfrastrukturprogramm des BMWF Forschungsprojekt Konsortium Hochleistungsrechnen, the German Science Foundation (DFG) through Grant number Zi 663/6-1, the Volkswagen Foundation (I/76 520), and the Austrian Science Foundation (FWF) through grants P18523-N16 and P19300-N16. In addition, the authors acknowledge the ESO Mobilitätsstipendien des BMWF (Austria), and the Tiroler Wissenschaftsfonds (Gefördert aus Mitteln des vom Land Tirol eingerichteten Wissenschaftsfonds). We thank Elif Kutdemir for fruitful discussions.

References

- Bamford, S. P., Milvang-Jensen, B., Aragón-Salamanca, A., & Simard, L. 2005, *MNRAS*, 361, 109
- Böhm, A., Ziegler, B. L., Saglia, R. P., et al. 2004, *A&A*, 420, 97
- Chemin, L., Balkowski, C., Cayatte, V., et al. 2006, *MNRAS*, 366, 812
- Duc, P.-A., Brinks, E., Springel, V., et al. 2000, *AJ*, 120, 1238
- Epinat, B., Amram, P., & Balkowski, C. 2006, *IAU Symp.*, 235,
- Flores, H., Hammer, F., Puech, M., Amram, P., & Balkowski, C. 2006, *A&A*, 455, 107
- Ganda, K., Falcón-Barroso, J., Peletier, R. F., et al. 2006, *MNRAS*, 367, 46
- Garrido, O., Marcelin, M., Amram, P., & Boulesteix, J. 2002, *A&A*, 387, 821
- Genzel, R., et al. 2006, *Nature*, 442, 786
- Jäger, K., Ziegler, B. L., Böhm, A., et al. 2004, *A&A*, 422, 907
- Jesseit, R., Naab, T., Peletier, R. F., & Burkert, A. 2007, *MNRAS*, 376, 997
- Kapferer, W., Knapp, A., Schindler, S., Kimeswenger, S., & van Kampen, E. 2005, *A&A* 438, 87
- Kapferer, W., Kronberger, T., Schindler, S., Ziegler, B. L., & Böhm A. 2006, *A&A*, 446, 847
- Krajnović, D., Cappellari, M., de Zeeuw, P. T., & Copin, Y. 2006, *MNRAS*, 366, 787
- Kronberger, T., Kapferer, W., Schindler, S., et al. 2006, *A&A*, 458, 69
- Kutdemir, E., Ziegler, B., & Peletier, R. F. 2007, *IAU Symp.*, 241 [arXiv:astro-ph/0701918]
- Mo, H. J., Mao, S., & White, S. D. M. 1998, *MNRAS*, 295, 319
- Nakamura, O., Aragón-Salamanca, A., Milvang-Jensen, B., et al. 2006, *MNRAS*, 366, 144
- Pierce, M. J., & Tully, R. B. 1992, *ApJ*, 387, 47
- Portinari, L., & Sommer-Larsen, J. 2007, *MNRAS*, 375, 913
- Springel, V. 2005, *MNRAS*, 364, 1105
- Springel, V., & Hernquist, L. 2003, *MNRAS*, 333, 649
- Springel, V., Di Matteo, T., & Hernquist, L. 2005, *MNRAS*, 361, 776
- Vogt, N. P. 2001, in *ESO astrophysics symposia, Deep Fields*, ed. S. Cristiani, A. Renzini, & R. E. Williams (Springer), 112
- Ziegler, B. L., Böhm, A., Fricke, K. J., et al. 2002, *ApJ*, 564, L69
- Ziegler, B. L., Böhm A., Jäger, K., Heidt, J., & Möllenhoff, C. 2003, *APJ*, 598, L87
- Ziegler, B., et al. 2006, *IAU Symp.*, 235